The Innovation

Report

Enhanced catalytic performance of Pt by coupling with carbon defects

Yan Dong,[1,3] Yuan Wang,[1] Ziqi Tian,[1,2] Kemin Jiang,[1,2] Yanle Li,[1,2,*] Yichao Lin,[1,2] Colin W. Oloman,[3] Elod L. Gyenge,[3] Jianwei Su,[1,4,*] and Liang Chen[1,2,*]

*Correspondence: liyanle@nimte.ac.cn (Y.L.); sujianwei@nimte.ac.cn (J.S.); chenliang@nimte.ac.cn (L.C.)

Received: March 23, 2021; Accepted: August 27, 2021; Published Online: September 2, 2021; https://doi.org/10.1016/j.xinn.2021.100161

Graphical abstract

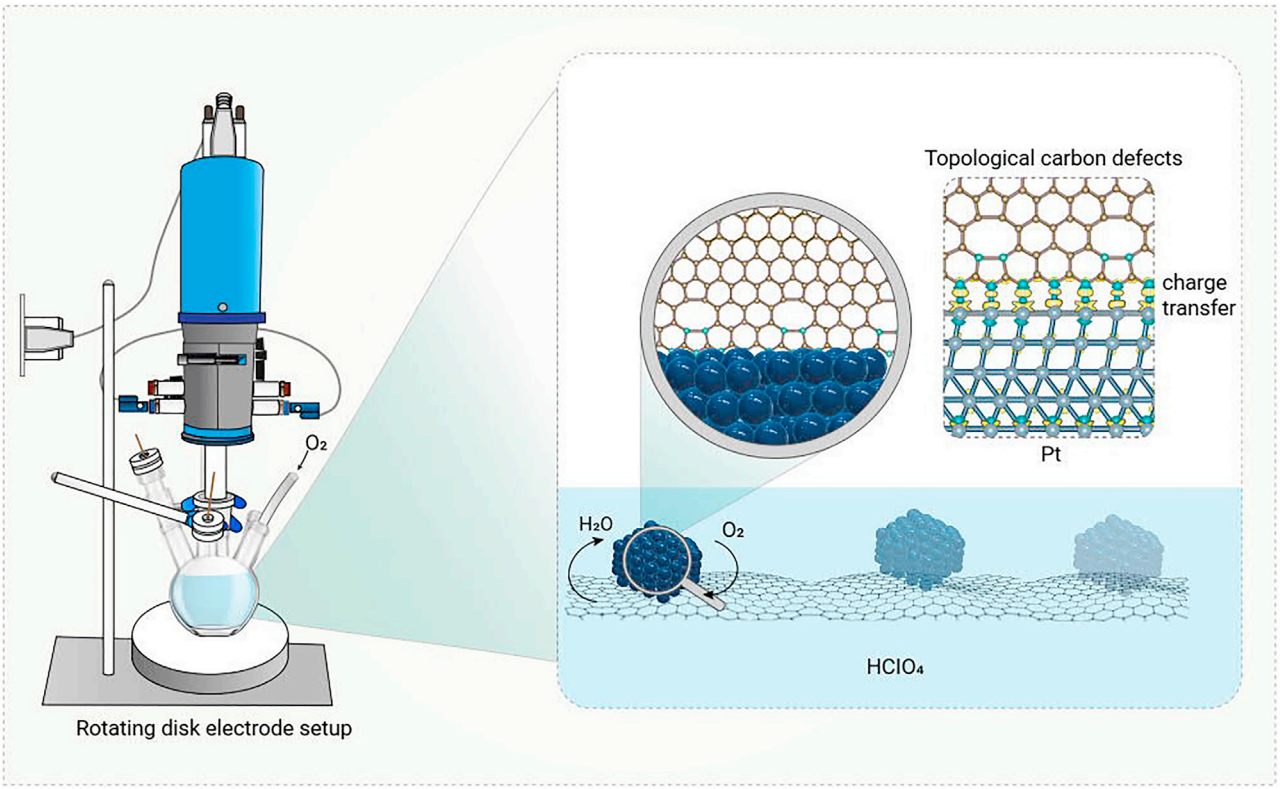

Public summary

- A novel method to obtain topologically defective porous carbon particles is proposed
- Pt nanoparticles are deposited on the topological carbon defects of porous carbon
- The interaction between Pt particles and carbon defects can adjust d-band center position
- Pt-DPC shows much better ORR performance than that of commercial Pt/C

Report

Enhanced catalytic performance of Pt by coupling with carbon defects

Yan Dong,[1,3] Yuan Wang,[1] Ziqi Tian,[1,2] Kemin Jiang,[1,2] Yanle Li,[1,2,*] Yichao Lin,[1,2] Colin W. Oloman,[3] Elod L. Gyenge,[3] Jianwei Su,[1,4,*] and Liang Chen[1,2,*]

[1]Ningbo Institute of Materials Technology and Engineering, Chinese Academy of Sciences, Ningbo 315201, China

[2]University of Chinese Academy of Sciences, Beijing 100049, China

[3]Department of Chemical and Biological Engineering, Clean Energy Research Center (CERC), The University of British Columbia, Vancouver V6T 1Z3, Canada

[4]Institutes of Physical Science and Information Technology, Key Laboratory of Structure and Functional Regulation of Hybrid Materials (Ministry of Education), Anhui University, Hefei, Anhui 230601, China

*Correspondence: liyanle@nimte.ac.cn (Y.L.); sujianwei@nimte.ac.cn (J.S.); chenliang@nimte.ac.cn (L.C.)

Received: March 23, 2021; Accepted: August 27, 2021; Published Online: September 2, 2021; https://doi.org/10.1016/j.xinn.2021.100161

Citation: Dong Y., Wang Y., Tian Z., et al., (2021). Enhanced catalytic performance of Pt by coupling with carbon defects. The Innovation **2(4)**, 100161.

Defect engineering is a promising strategy for supported catalysts to improve the catalytic activity and durability. Here, we selected the carbon (C) matrix enriched with topological defects to serve as the substrate material, in which the topological defects can act as anchoring centers to trap Pt nanoparticles for driving the O_2 reduction reactions (ORRs). Both experimental characterizations and theoretical simulations revealed the strong Pt-defect interaction with enhanced charge transfer on the interface. Despite a low Pt loading, the supported catalyst can still achieve a remarkable 55 mV positive shift of half-wave potential toward ORR in O_2-saturated 0.1 M $HClO_4$ electrolyte compared with the commercial Pt catalyst on graphitized C. Moreover, the degeneration after 5,000 voltage cycles was negligible. This finding indicates that the presence of strong interaction between Pt and topological C defects can not only stabilize Pt nanoparticles but also optimize the electronic structures of Pt/C catalysts toward ORR.

Keywords: O_2 reduction reaction; Pt-based catalysts; topological C defects; metal-support interactions; proton-exchange-membrane fuel cells

INTRODUCTION

Proton-exchange-membrane fuel cells (PEMFCs) have been deemed as a promising sustainable and environmental-benign energy conversion technology with great potential to mitigate environmental deterioration and the energy crisis.[1,2] In general, a PEMFC system comprises two half-reactions: O_2 reduction reaction (ORR) on its cathode and hydrogen oxidation reaction (HOR) on its anode. However, cathodic ORR is a kinetically sluggish reaction involving multiple electron transfer processes. Therefore, lacking efficient ORR electrocatalysts in acidic media is one of the main bottlenecks for commercial application of PEMFCs. Platinum (Pt) is universally regarded as the most advanced catalyst toward ORR in acidic media. To date, the development of PEMFCs is still highly dependent on the Pt-based catalysts; however, its scarcity and high price hinder large-scale commercialization.[3]

In recent decades, extensive efforts have been paid to exploring inexpensive alternatives to take the place of Pt-based catalysts. Unfortunately, catalytic performances of the nonprecious catalysts are still far away from the requirement for replacing Pt-based catalysts. Another potentially feasible strategy is to develop cost-effective catalysts with low Pt contents for maintaining good balance between performance and cost. In order to boost the atom utilization efficiency (AUE) of Pt, C materials are widely applied as the support materials, including graphene-based materials, C black, C gels, C nanotubes (CNTs), and ordered mesoporous C.[4] Indeed, C materials have many advantages as electrocatalyst supports in terms of impressive electrical conductivity, super-high specific surface area, acceptable chemical stability in harsh environment, and abundant natural resources.[5] For the low Pt-content catalysts supported by C substrates, the interaction between Pt and C substrates not only allows the fine dispersion and immobilization of Pt nanoparticles but also adjusts the morphology of Pt nanoparticles.[4] Aside from the geometric effect, the electronic effect arising from Pt-C supports interactions plays a vital role in the improvement of ORR performance for Pt-based catalysts. Indeed, the electron transfer from Pt to support materials may tune the system's Galvani potential, lower the Fermi level of the system, and increase the electronic density of Pt nanoparticles.[6,7] As a result, the modified electronic properties of Pt particles would benefit both the electrochemical catalytic activity and stability.[4]

Currently, defect engineering is widely used to tune the electronic structures of catalysts, and has the potential to overcome the intrinsic drawback and hence enhance the catalytic performance dramatically.[8] This strategy can also be extended to the design of catalyst supports in order to enhance the electronic interaction with metal catalysts.[9] Very recently, topological defects in C materials have attracted increasing attention as the catalytic sites toward multiple electrochemical reactions.[10,11] For example, Yao and coworkers reported that the edged pentagon defects can serve as the robust active centers toward ORR in acidic media.[10] Our recent work reported a high-performance CO_2 electroreduction catalyst of porous C enriched with high-density topological defects, which were created by the N-elimination process under ammonia thermal treatment.[12] We note that the topological defects, especially 5-member-ring C defects, exhibit the dramatically increased coordination effect with metal atoms similar to the metallocene analogues, which may serve as the anchor centers for trapping metal particles by the strong binding energy with enhanced charge transfer.[13] Thus, we conceive that the prepared three-dimensional topologically defective porous C particles (DPCs) can be applied as substrates to support and stabilize Pt nanoparticles to achieve high Pt AUE and enhanced ORR catalytic activity.

In our work, Pt nanoparticles were successfully dispersed onto the DPC supports uniformly by using friendly reducing agents. The prepared Pt-DPC catalysts showed a great half-wave potential of 0.91 V versus reversible hydrogen electrode (RHE) in 0.1 M $HClO_4$ electrolyte, which is 55 mV higher potential than commercial Pt-C. Moreover, the superior activity can be well maintained during accelerated durability test (ADT) of 5,000 cyclic voltammetry (CV) cycles. Density functional theory (DFT) calculations revealed that the performance of ORR in acidic media was promoted by the electronic interaction between Pt nanoparticles and topological defects.

RESULTS AND DISCUSSION

In Figure 1, the schematic diagram illustrates the preparation procedure for Pt-DPC catalysts. Here, Pt-DPC was facilely synthesized via a two-step method (see the experimental section in supplemental information). Firstly, DPC particles were synthesized following our previously reported method.[12] Briefly, DPC particles were obtained by carbonization of zeolitic imidazolate framework (ZIF)-8 precursor (Figure S1) and acid etching, followed with NH_3 thermal treatment to remove pyridine and pyrrole nitrogen for creating topological defects in C matrix.[12,14] The as-prepared DPC shows a mean

Report

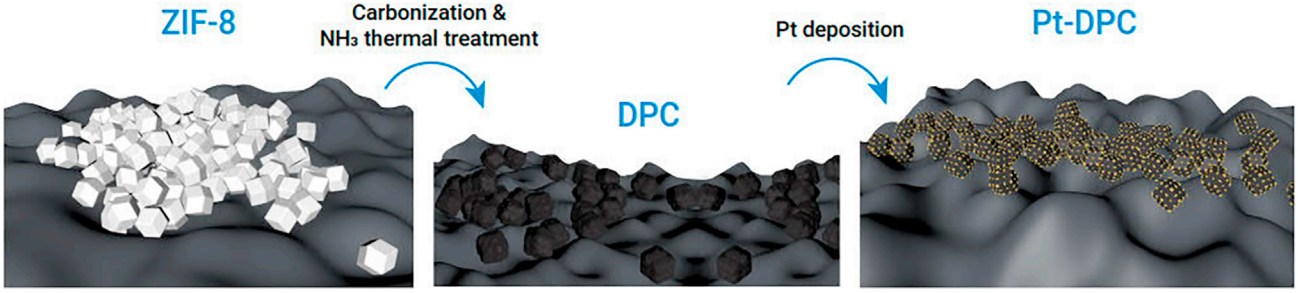

Figure 1. Schematic illustration of synthetic route of Pt-DPC catalysts

diameter of approximately 100 nm with a polyhedron-like structure in the field-emission scanning electron microscopy (FESEM) image (Figures 2A and S3). It is notable that the N content sharply decreased from 20.33 atom % (N-enriched porous C [NPC]; Figures S2, S4, and S5) to 2.23 atom % (DPC) according to the X-ray photoelectron spectroscopy (XPS) data in Table S1 and Figure S2C. The accelerating removal of N atoms could produce a large amount of dangling C bonds, thus yielding a high content of topological defects by the rotation and rearrangement of these C dangling bonds.[12,15] In Figure S2B, DPC showed the highest value of the intensity ratio between the disorder-induced D bond and the G band (I_D/I_G), indicating highest density of defects in DPC among these samples.[16,17] However, XPS results indicated the lowest N content in DPC. Therefore, it could be inferred that a large number of topological C defects had been created in DPC during ammonia thermal treatment.[12]

Pt nanoparticles were uniformly grown on the DPC particles (Figure 1), in which ethylene glycol (EG), a mild and environmentally friendly reducing agent, was used to reduce Pt nanoparticles via refluxing. As shown in Figure 2B, the obtained Pt-DPC still maintained the polyhedron-like structure with mean sizes of about 100 nm. Besides, the representative transmission electron microscopy (TEM) image shows that Pt nanoparticles were uniformly dispersed on DPC with a mean diameter of approximately 3–4 nm, similar to that of Pt nanoparticles on the commercial Pt-C in Figure 2C. The high-resolution TEM (HRTEM) image of Pt-DPC (Figure 2D) displays three sets of lattice fringes with spacings of 0.23, 0.20, and 0.14 nm, corresponding to the (111), (200), and (220) facets planes of the face-centered cubic (FCC) Pt phase, respectively. In Figures 2E–2H, the high-angle annular dark-field scanning TEM (HAADF-STEM) image and corresponding energy-dispersive X-ray spectroscopy (EDX) mappings display a homogeneous distribution of Pt, N, and C over the C supports. In order to better understand the influence of topological C defects, the NPC and ZIF-8-NH_3 were also prepared as the reference C supports. The NPC contained barely topological C defects but high concentration of nitrogen dopants, whereas ZIF-8-NH_3 (Figures S6 and S7) had similar nitrogen content with DPC but much lower topological C defects.[12] In contrast to Pt-NPC and Pt-ZIF-8-NH_3 samples (Figures S8–S11), Pt nanoparticles on the DPC show a smaller mean size and a more uniform dispersion, which is attributed to excellent anchoring effect of the topological defects in C supports. For Pt-NPC and Pt-ZIF-8-NH_3 obtained from a similar amount of Pt precursor, insufficient strong anchoring sites may account for the inhomogeneous distribution of Pt nanoparticles.[13,18] These results were also consistent with the further measurement of Pt mass loading by the inductively coupled plasma optical emission spectroscopy (ICP-OES). Indeed, Pt-DPC had a higher loading amount of Pt than Pt-NPC and Pt-ZIF-8-NH_3 according to the ICP-OES data (Table S6). However, the Pt mass loadings of these three samples were all less than the amount of 20 wt % in the commercial Pt-C. Besides, Pt-DPC exhibited the high Brunauer-Emmett-Teller (BET) surface area of 870.2 $m^2\ g^{-1}$ among the prepared catalysts of Pt nanoparticles supported on various defective C substrates listed in Tables S2 and S3 (Figure S12). Apparently, the high specific surface area could

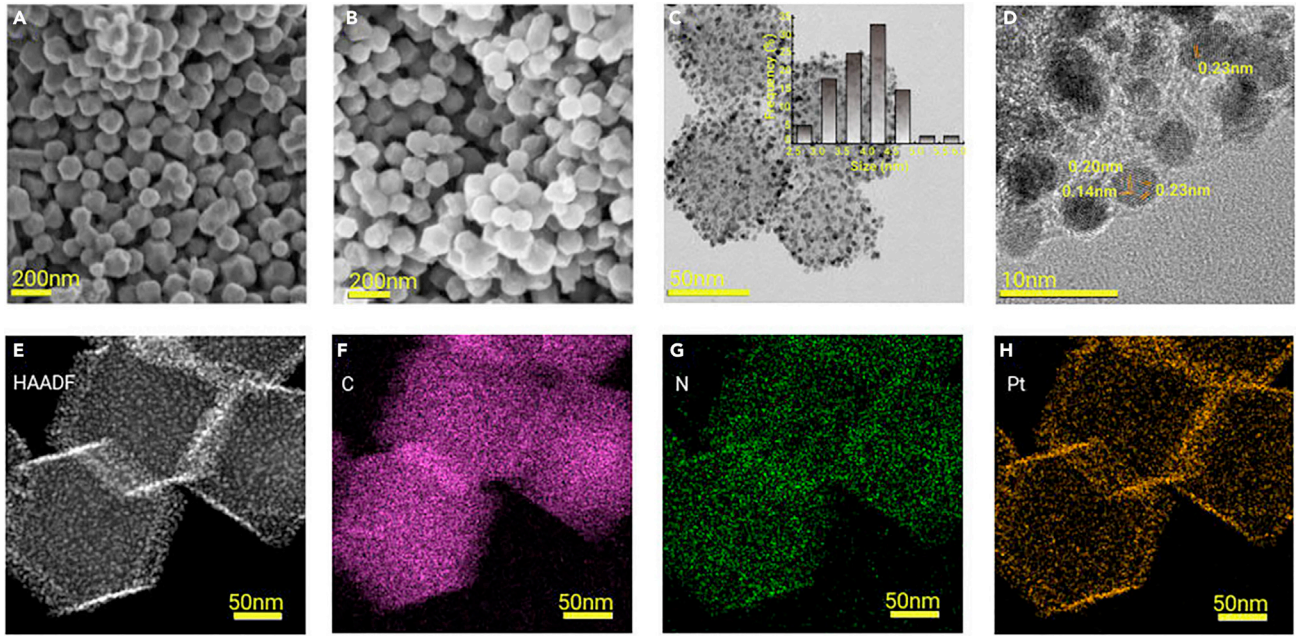

Figure 2. Morphology and structure of DPC and Pt-DPC (A) FESEM image of DPC nanoparticles. (B) FESEM image of Pt-DPC. (C) TEM image of Pt-DPC. (D) HRTEM image of Pt-DPC. (E–H) HAADF-STEM image and EDX maps of different elements for Pt-DPC, C (F), N (G), and Pt (H).

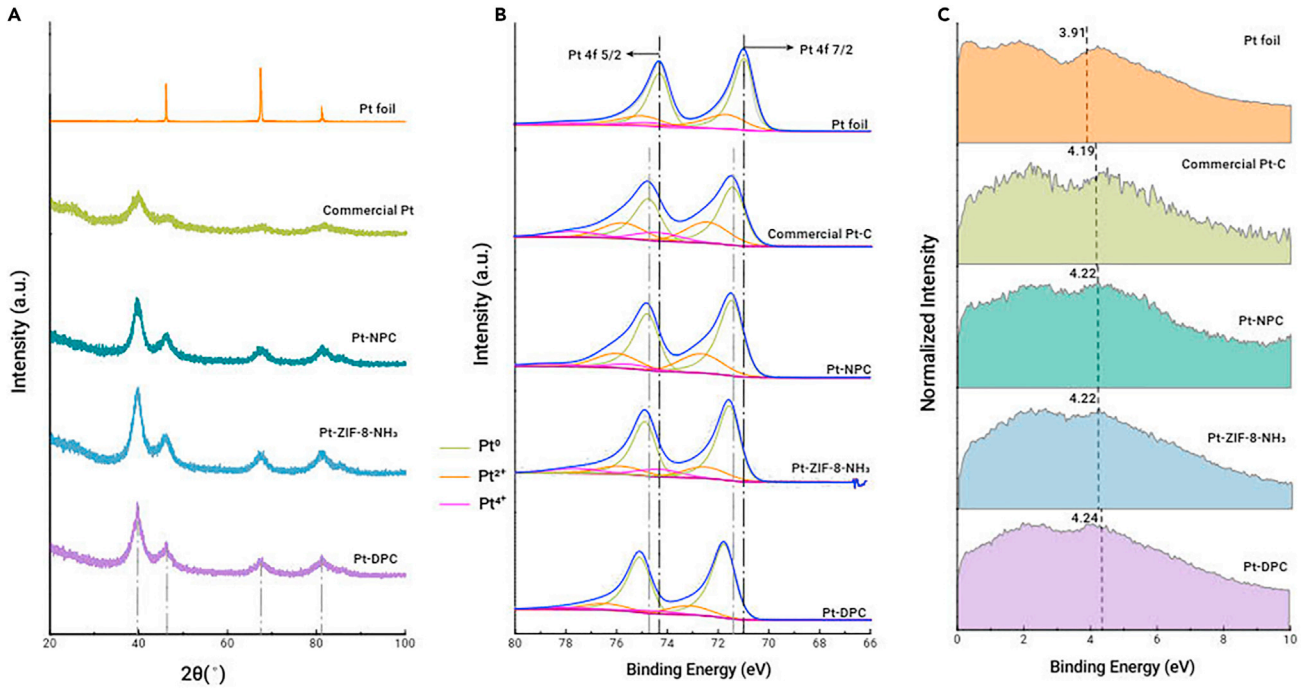

Figure 3. Spectroscopic characterization (A) XRD results of Pt foil, commercial Pt-C, Pt-NPC, Pt-ZIF-8-NH_3, and Pt-DPC. (B) Valance bond results of Pt foil, commercial Pt-C, Pt-NPC, Pt-ZIF-8-NH_3, and Pt-DPC. (C) XPS results of Pt 4f of Pt foil, commercial Pt-C, Pt-NPC, Pt-ZIF-8-NH_3, and Pt-DPC.

provide more active centers, which may improve the catalytic activity toward ORR.

All obtained samples display four diffraction peaks at 2θ of 39.76°, 46.24°, 67.45°, and 81.41° in Figure 3A, which correspond to (111), (200), (220), and (311) facets of Pt FCC phase (Joint Committee on Powder Diffraction Standards [JCPDS] card no. 04-0802), respectively.[19] Clearly, this result is consistent with the HAADF-STEM data. The average size of Pt nanoparticles was 4 nm for Pt-DPC, which is also consistent with TEM results. We next used XPS to investigate the oxidation state of the Pt surface. Figure 3B exhibits the high-resolution XPS results of Pt 4f for commercial Pt-C, Pt-NPC, Pt-ZIF-8-NH_3, and Pt-DPC. The Pt 4f spectra clearly contain two peaks, corresponding to Pt 4f 7/2 and Pt 4f 5/2 states, due to the spin orbital splitting.[20] The two peaks can be deconvoluted into three pairs of doublets peaks according to different Pt oxidation states (Pt^0, Pt^{2+}, and Pt^{4+}). The values of each peak are listed in Tables S4 and S5. Commonly, Pt^0 has been identified as the predominant oxidation state in Pt catalysts. Note that Pt foil, as a reference sample, exhibits the lowest values for the Pt^0 peak positions among all Pt-based catalysts. For the other four samples with C support, there are positive shifts of the Pt^0 peaks following the trend of commercial Pt-C < Pt-NPC < Pt-ZIF-8-NH_3 < Pt-DPC, implying the electrons transfer from Pt nanoparticles to C substrates.[21,22] It has been reported that the N heteroatoms can intensify electron transfers from Pt particles to C supports.[19,23] However, we found that such effect is moderate so that Pt-NPC with the highest N content (20.33 atom %) only exhibits a slight positive shift. In comparison, the electron-withdrawing effect of topological C defects is more profound. As a result, the largest positive shift of Pt 4f in the binding energy (BE) was shown for Pt-DPC (0.3 eV). The strong binding energy between Pt nanoparticles and DPC modified the core-level f-band of Pt and effectively restricted the migration of Pt, which would certainly have some influence on the catalytic activity and enhance the stability compared with commercial Pt-C.[21,24] It is well accepted that the d-band center (ϵ_d) relative to Fermi level (E_f) is a key factor that determines the intrinsic ORR catalytic activity of Pt-based catalysts[25,26] In general, the moving away of the d-band center from the Fermi level is associated with the weakened binding with O-containing species and the improved ORR activity. We have thus measured the valence band spectra (VBS) for these five samples. As shown in Figure 3C, the ϵ_d was found to be 3.91, 4.19, 4.22, 4.22, and 4.24 eV for Pt foil, commercial Pt-C, Pt-NPC, Pt-ZIF-8-NH_3, and Pt-DPC, respectively, indicating that the d-band centers can be tailored by the interaction between Pt and C supports. Indeed, DPC with the strongest electron-withdrawing effect shows the largest shift of the Pt d-band center.

To evaluate the electrocatalytic ORR performance, CV curves were obtained in O_2- and Ar-saturated 0.1 M $HClO_4$ electrolyte using a typical three-electrode configuration (Figures 4A and S13). The *H-adsorption/desorption peaks are usually shown between 0.1 and 0.4 V, while the O*/OH*-adsorption/desorption peaks are observed between 0.8 and 1.1 V.[27] Compared with the curve in Ar-saturated solution, the Pt-DPC displayed a remarkable ORR catalytic activity with the cathodic peak of ORR at 0.91 V versus RHE in O_2-saturated electrolyte (Figure 4A). In addition, linear sweep voltammetry (LSV) was carried out on a rotating disk electrode (RDE) at 1,600 rpm in O_2-saturated 0.1 M $HClO_4$ electrolyte at 25°C to investigate the ORR activity and the kinetics of the prepared catalysts. Figure 4B clearly displays the LSV curves of Pt-DPC, Pt-NPC, Pt-ZIF-8-NH_3, commercial Pt-C, and DPC. The values of half-wave potential, as an indicator of ORR activity, increase in the order of DPC, commercial Pt-C, Pt-NPC, Pt-ZIF-8-NH_3, and Pt-DPC. Note that the pristine DPC shows poor activity toward ORR with a low half-wave potential at 0.56 V versus RHE. By comparison, the Pt-DPC catalyst shows the best ORR performance with a 55 mV higher half-wave potential than that of commercial Pt-C. Furthermore, Pt-DPC shows a much smaller value of Tafel slope (90 mV dec^{-1}) than all the other samples (Figures 4C, S15, and S16), which indicates the enhanced kinetics of Pt-DPC toward ORR. These results further confirmed that the electronic structure of Pt nanoparticles could be modified by topological C defects in C supports, which can be beneficial to the improvement of the activity and kinetics of Pt toward ORR. The electrochemical active surface area (ECSA) can be obtained by using the hydrogen underpotential deposition method. As seen in Figures 4D and S14 and Table S7, Pt-DPC displays the highest ECSA of 76.47 m^2g^{-1}, implying the highest density of active sites. This further proves the excellent anchoring effect of topological C defects, as mentioned before. Pt-DPC achieved the ORR mass activity of 98.54 mA mg^{-1}_{Pt}, which is 2.42 times that of commercial Pt at 0.9 V versus RHE in Table S8. The surface activity (SA) also follows the trend of commercial Pt-C < Pt-

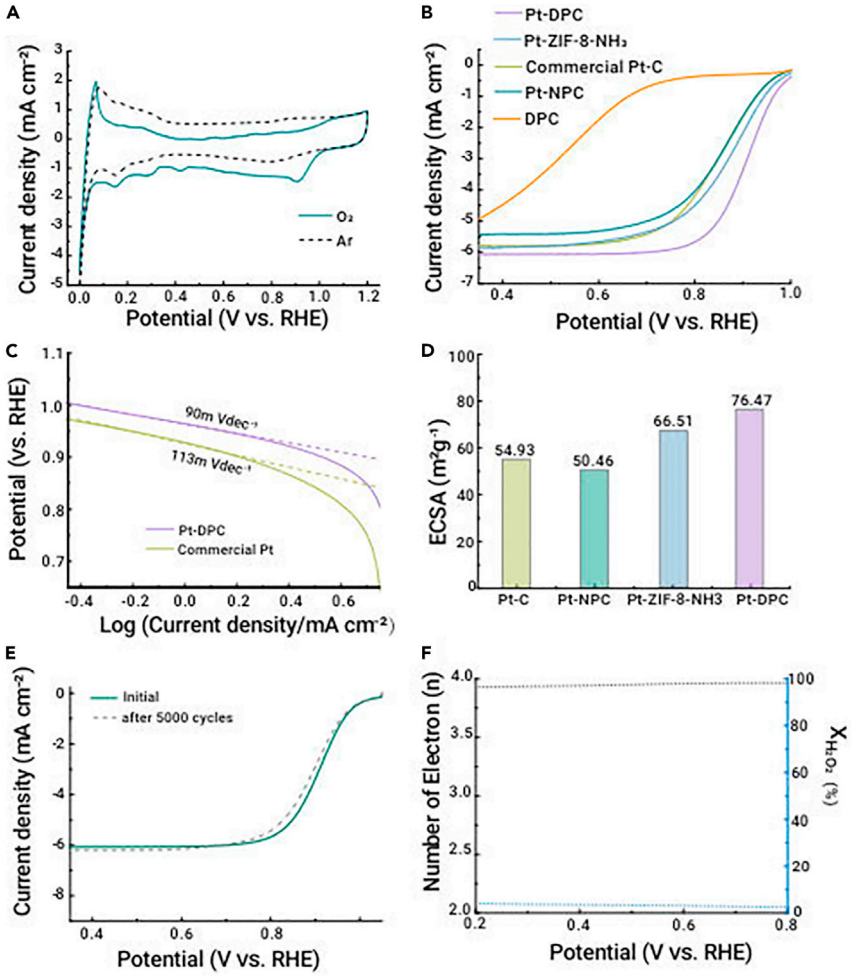

Figure 4. Electrochemical performance (A) CV curves of Pt-DPC performed in O_2- and Ar-saturated 0.1 M $HClO_4$ electrolyte.
(B) LSV curves of Pt-DPC, Pt-ZIF-8-NH_3, DPC, Pt-NPC, and commercial Pt-C at 1,600 rpm.
(C) Tafel plots for Pt-DPC and commercial Pt-C.
(D) The ECSA of Pt-DPC, Pt-ZIF-8-NH_3, Pt-NPC, and commercial Pt-C.
(E) ORR polarization curves of Pt-DPC before and after 5,000 cycles.
(F) Electron transfer number (n) and FE_{H2O2} for Pt-DPC in O_2-saturated 0.1 M $HClO_4$ electrolyte.

NPC < Pt-ZIF-8-NH_3 < Pt-DPC, indicating that the enhanced intrinsic activity of Pt catalysts is attributed to the interaction between Pt nanoparticles and topological C defects.

Stability is also a critical parameter for commercial application of ORR catalysts. We further investigated the durability of the Pt catalysts by an ADT under CV scanning between 0.6 and 1.1 V versus RHE in O_2-saturated 0.1 M $HClO_4$ electrolyte. Figures 4E and S17 show the polarization curves of Pt-DPC and commercial Pt-C before and after ADTs. After 5,000 cycles of ADTs, the polarization curves of Pt-DPC show superior durability with a negligible shift decay (<1 mV). No significant difference could be found from the results of TEM, X-ray diffraction (XRD), and XPS (Figures S20–S22) after ADT, which also indicated the stability of Pt-DPC. By comparison, the commercial Pt-C exhibits a 7 mV loss under the same conditions. Intrinsically, the deterioration of catalytic activity can be attributed to the leaching and aggregation process of metal catalyst.[28] For Pt-DPC, the strong binding energy between Pt nanoparticles and topological C defects restricted the migration of Pt atoms during ORR process, which could slow down the loss rate of ORR activity. Faradaic efficiency (FE) of H_2O_2 generation and electron transfer number (n) can be calculated from the ring-disk currents in order to investigate the ORR pathways. The number of electron transfer is about 3.95 for sample Pt-DPC in the range between 0.2 and 0.8 V versus RHE in Figure 4F. The FE of H_2O_2 production is below 5%.[29–32] This result confirmed a transfer reaction of almost four electrons during the ORR process.[33]

Finally, we performed DFT calculations to understand the influence of the Pt-C interface and topological defects on the ORR process. As shown in the aforementioned experiments, the mean diameter of Pt nanoparticles was found to be approximately 3–4 nm. Herein we constructed an interface model instead of the sub-nano cluster model supported on C where the Pt cluster is too small to represent the realistic Pt-C interface. As shown in Figure 5A and 5B, a C layer was vertically placed on the surface of a Pt slab containing five layers. Four different edges of the C layer were considered, labeled as C-edge, N-edge, 5775-edge, and 585-edge, respectively. Note that 585- and 5775-motifs are two commonly investigated topological defects as the key structures in many electrocatalytic systems.[12,17,34] We first calculated the surface charge distribution based on the Bader charge analysis. Due to the low coordination number of the outermost Pt atoms, the Pt surface possesses more electrons than in the bulk. However, electrons would transfer from Pt to the C layer once the chemical/coordination bonds are formed, particularly in the case of 585-edge ring motif, which is in good agreement with the XPS results. According to the Hückel rule, the five-membered ring structure tends to accept electrons to achieve a stable electronic state. In other words, these topological defects exhibit a more electron-withdrawing nature than the six-membered-ring Cs in the pristine graphitic structures. As a result, the partial charges of Pt surface with the 585- and 5775-motifs are more positive than that of pristine C-edge. Figure 5D displays the deformation charge density of the model containing the 585-defect, clearly illustrating the charge transfer from metal to the interface. Previous studies revealed that Pt binds O too strongly, thus the overall ORR reaction rate is determined by the reductive desorption step of OH groups.[35,36] Herein, upon the chemical interaction with 585- and 5775-motifs, the Pt surface with fewer electrons has difficulty reducing O_2 to form *OH. Conversely, the desorption of *OH is promoted according to the well-established scaling relationship.[37]

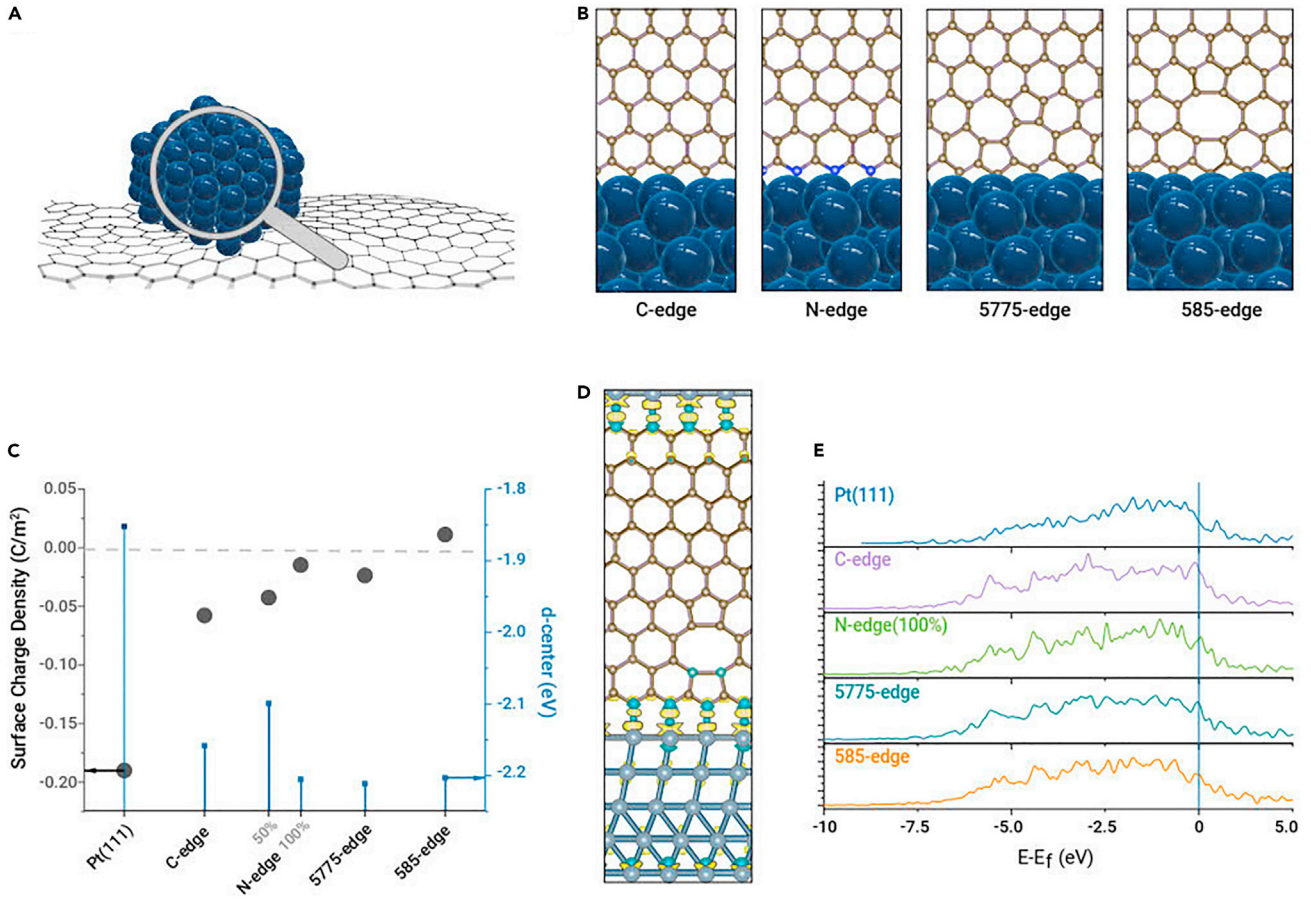

Figure 5. DFT calculations (A) The schematic diagram of the studied system. (B) The models of covalent interfaces between Pt (111) facet and the C layers with various edges. (C) The comparison of surface charge density and d-band center before and after the covalent interface formation. (D) The charge density difference of the system composed of Pt (111) and 585-edge with the isosurface of 0.005 eÅ^{-3}. The cyan and yellow represent electron depletion and increase area, respectively. (E) The projected DOSs (pDOSs) of *d*-orbitals of the Pt atoms in the surface layers.

Moreover, we plotted the projected densities of states (DOSs) of d-band in each model in Figure 5E and located the band center in Figure 5C. It is found that the d-band center of the Pt surface downshifts significantly upon the chemical interaction with the C layer, which is consistent with our experimental VBS results.[35,38] In comparison, the d-band center positions of Pt-NPC and Pt-ZIF-8-NH_3 are between that of commercial Pt-C and Pt-DPC, which indicated that topological C defects could be more effective in regulating the d-band center of Pt. A similar trend has also been observed in alloy systems in which the downshift d-band center is related to the weakened binding to the O-containing species and the improved ORR activity.[39,40] Therefore, the electronic structure of the Pt surface is well modulated by introducing the C-Pt interface and the topology defect. The d-band center position of Pt can be adjusted in the presence of abundant topological C defects in C substrates, which contributes to higher activity for ORR and higher durability in harsh electrochemical processes.

Conclusions

In summary, we show that ORR performance of Pt can be controlled by tuning the interaction between Pt nanoparticles and C supports. In particular, the topological C defects with stronger electron-withdrawing nature can alter the d-band structure of the Pt nanoparticles and weaken the adsorption energy of intermediates produced during ORR much more profoundly than the graphitic C and N-doped C. Thus, a significantly enhanced catalytic activity and durability toward ORR in acidic solutions can be achieved (Table S9). This work offers a promising strategy for the design of highly active and durable catalysts in ORR and other electrochemical reactions by using the coupling interaction between metal and C supports with appropriate functionalities.

REFERENCES

1. Ren, X., Lv, Q., Liu, L., et al. (2020). Current progress of Pt and Pt-based electrocatalysts used for fuel cells. Sustain. Energy Fuels ***4***, 15–30.
2. Yuan, Y., Adimi, S., Thomas, T., et al. (2021). Co3Mo3N—an efficient multifunctional electrocatalyst. The Innovation ***2***, 10096.
3. Ding, H., Wang, S., Long, Y., and Chan, S.H. (2021). Non-aqueous solution synthesis of Pt-based nanostructures for fuel cell catalysts. Mater. Today Energy ***19***, 100616.
4. Antolini, E. (2009). Carbon supports for low-temperature fuel cell catalysts. Appl. Catal. B - Environ. ***88***, 1–24.
5. Sui, S., Wang, X., Zhou, X., et al. (2017). A comprehensive review of Pt electrocatalysts for the oxygen reduction reaction: nanostructure, activity, mechanism and carbon support in PEM fuel cells. J. Mater. Chem. A. ***5***, 1808–1825.
6. Yu, X., and Ye, S. (2007). Recent advances in activity and durability enhancement of Pt/C catalytic cathode in PEMFC. J. Power Sourc. ***172***, 133–144.
7. Jinnouchi, R., Toyoda, E., Hatanaka, T., and Morimoto, Y. (2010). First principles calculations on site-dependent dissolution potentials of supported and unsupported Pt particles. J. Phys. Chem. C ***114***, 17557–17568.
8. Yan, X., Jia, Y., and Yao, X. (2018). Defects on carbons for electrocatalytic oxygen reduction. Chem. Soc. Rev. ***47***, 7628–7658j.
9. Lim, D.-H., and Wilcox, J. (2012). Mechanisms of the oxygen reduction reaction on defective graphene-supported Pt nanoparticles from first-principles. J. Phys. Chem. C ***116***, 3653–3660.
10. Jia, Y., Zhang, L., Zhuang, L., et al. (2019). Identification of active sites for acidic oxygen reduction on carbon catalysts with and without nitrogen doping. Nat. Catal. ***2***, 688–695.
11. Tang, C., Wang, H.F., Chen, X., et al. (2016). Topological defects in metal-free nanocarbon for oxygen electrocatalysis. Adv. Mater. ***28***, 6845–6851.

12. Dong, Y., Zhang, Q., Tian, Z., et al. (2020). Ammonia thermal treatment toward topological defects in porous carbon for enhanced carbon dioxide electroreduction. Adv. Mater. e2001300.
13. Zhang, L., Jia, Y., Gao, G., et al. (2018). Graphene defects trap atomic Ni species for hydrogen and oxygen evolution reactions. Chem ***4***, 285–297.
14. Zheng, F., Yang, Y., and Chen, Q. (2014). High lithium anodic performance of highly nitrogen-doped porous carbon prepared from a metal-organic framework. Nat. Commun. ***5***, 5261.
15. Banhart, F., Kotakoski, J., and Krasheninnikov, A.V. (2011). Structural defects in graphene. ACS Nano ***5***, 26–41.
16. Jia, Y., Zhang, L., Zhuang, L., et al. (2019). Identification of active sites for acidic oxygen reduction on carbon catalysts with and without nitrogen doping. Nat. Catal. ***2***, 688–695.
17. Jia, Y., Zhang, L., Du, A., et al. (2016). Defect graphene as a trifunctional catalyst for electrochemical reactions. Adv. Mater. ***28***, 9532–9538.
18. Cheng, Q., Hu, C., Wang, G., et al. (2020). Carbon-defect-driven electroless deposition of Pt atomic clusters for highly efficient hydrogen evolution. J. Am. Chem. Soc. ***142***, 5594–5601.
19. Qiao, Z., Hwang, S., Li, X., et al. (2019). 3D porous graphitic nanocarbon for enhancing the performance and durability of Pt catalysts: a balance between graphitization and hierarchical porosity. Energy Environ. Sci. ***12***, 2830–2841.
20. Ma, J., Habrioux, A., Luo, Y., et al. (2015). Electronic interaction between platinum nanoparticles and nitrogen-doped reduced graphene oxide: effect on the oxygen reduction reaction. J. Mater. Chem. A. ***3***, 11891–11904.
21. Zhou, Y., Holme, T., Berry, J., et al. (2010). Dopant-induced electronic structure modification of HOPG surfaces implications for high activity fuel cell catalysts. J. Phys. Chem. C ***114***, 506–515.
22. Holme, T., Zhou, Y., Pasquarelli, R., and O'Hayre, R. (2010). First principles study of doped carbon supports for enhanced platinum catalysts. Phys. Chem. Chem. Phys. ***12***, 9461–9468.
23. Su, F., Tian, Z., Poh, C.K., et al. (2010). Pt nanoparticles supported on nitrogen-doped porous carbon nanospheres as an electrocatalyst for fuel cells. Chem. Mater. ***22***, 832–839.
24. Zhou, Y., Pasquarelli, R., Holme, T., et al. (2009). Improving PEM fuel cell catalyst activity and durability using nitrogen-doped carbon supports: observations from model Pt/Hopg systems. J. Mater. Chem. ***19***, 7830.
25. Stamenkovic, V.R., Mun, B.S., Arenz, M., et al. (2007). Trends in electrocatalysis on extended and nanoscale Pt-bimetallic alloy surfaces. Nat. Mater. ***6***, 241–247.
26. Greeley, J., Stephens, I.E., Bondarenko, A.S., et al. (2009). Alloys of platinum and early transition metals as oxygen reduction electrocatalysts. Nat. Chem. ***1***, 552–556.
27. Garlyyev, B., Kratzl, K., Ruck, M., et al. (2019). Optimizing the size of platinum nanoparticles for enhanced mass activity in the electrochemical oxygen reduction reaction. Angew. Chem. Int. Ed. ***58***, 9596–9600.
28. Zhang, C., Shen, X., Pan, Y., and Peng, Z. (2017). A review of Pt-based electrocatalysts for oxygen reduction reaction. Front. Energy ***11***, 268–285.
29. Dong, K., Lei, Y., Zhao, H., et al. (2020). Noble-metal-free electrocatalysts toward H_2O_2 production. J. Mater. Chem. A. ***8***, 23123–23141.
30. Liang, J., Wang, Y., Liu, Q., et al. (2021). Electrocatalytic hydrogen peroxide production in acidic media enabled by NiS_2 nanosheets. J. Mater. Chem. A. ***9***, 6117–6122.
31. Dong, K., Liang, J., Wang, Y., et al. (2021). Honeycomb carbon nanofibers: a superhydrophilic O_2-entrapping electrocatalyst enables ultrahigh mass activity for the two-electron oxygen reduction reaction. Angew. Chem. Int. Ed. ***60***, 10583–10587.
32. Xu, Z., Zhao, H., Liang, J., et al. (2020). Noble-metal-free electrospun nanomaterials as electrocatalysts for oxygen reduction reaction. Mater. Today Phys. ***15***, 100280.
33. Lu, B., Guo, L., Wu, F., et al. (2019). Ruthenium atomically dispersed in carbon outperforms platinum toward hydrogen evolution in alkaline media. Nat. Commun. ***10***, 631.
34. Daiyan, R., Tan, X., Chen, R., et al. (2018). Electroreduction of CO_2 to CO on a mesoporous carbon catalyst with progressively removed nitrogen moieties. ACS Energy Lett ***3***, 2292–2298.
35. Stamenkovic, V., Mun, B.S., Mayrhofer, K.J.J., et al. (2006). Changing the activity of electrocatalysts for oxygen reduction by tuning the surface electronic structure. Angew. Chem. ***118***, 2963–2967.
36. Liu, Z., Zhao, Z., Peng, B., et al. (2020). Beyond extended surfaces: understanding the oxygen reduction reaction on nanocatalysts. J. Am. Chem. Soc. ***142***, 17812–17827.
37. Calle-Vallejo, F., Martínez, J.I., García-Lastra, J.M., et al. (2012). Physical and chemical nature of the scaling relations between adsorption energies of atoms on metal surfaces. Phys. Rev. Lett. ***108***, 116103.
38. Jinnouchi, R., Toyoda, E., Hatanaka, T., and Morimoto, Y. (2010). First principles calculations on site-dependent dissolution potentials of supported and unsupported Pt particles. J. Phys. Chem. C ***114***, 17557–17568.
39. Kitchin, J.R., Nørskov, J.K., Barteau, M.A., and Chen, J.G. (2004). Modification of the surface electronic and chemical properties of Pt(111) by subsurface 3d transition metals. J. Chem. Phys. ***120***, 10240–10246.
40. Stamenkovic, V.R., Mun, B.S., Arenz, M., et al. (2007). Trends in electrocatalysis on extended and nanoscale Pt-bimetallic alloy surfaces. Nat. Mater. ***6***, 241–247.

ACKNOWLEDGMENTS

This work was supported by National Natural Science Foundation of China (nos. 52002378 and 51872306), Natural Science Foundation of Zhejiang Provincial (nos. LQ19B030002, LD21E020001, and LY21B030006), the From 0 to 1 Innovative program of CAS (no. ZDBS-LY-JSC021), K. C. Wong Education Foundation (GJTD-2019-13), Ningbo S&T Innovation 2025 Major Special Program (nos. 2019B10046, 2020Z059, 2020Z107, and 2019B10041), and Ningbo Natural Science Foundation (no. 2019A610019).

AUTHOR CONTRIBUTIONS

Conceptualization, methodology, validation, data curation, formal analysis, and writing – original draft, Y.D.; conceptualization, DFT calculation, data curation, and formal analysis, Y.W. and Z.T. conceptualization, data curation, and formal analysis, K.J. writing – review & editing, and funding acquisition, Y.L. conceptualization and writing – review & editing, C.W.O. and E.L.G. conceptualization, resources, supervision, project administration, funding acquisition, and writing – review & editing, J.S. and L.C.

DECLARATION OF INTERESTS

The authors declare no competing financial interests.

SUPPLEMENTAL INFORMATION

Supplemental information can be found online at https://doi.org/10.1016/j.xinn.2021.100161.

LEAD CONTACT WEBSITE

https://liangchen.nimte.ac.cn/